Efficient Computation of the Pre-Asymptotic Behaviour of Unstable Two-Phase Flow Problems

W. A. Mulder

Shell Research B.V., Koninklijke/Shell, Exploratie en Productie Laboratorium, Postbus 60, 2280 AB Rijswijk, The Netherlands

A numerical method for studying the evolution towards the asymptotic solution of two-dimensional, two-phase displacement through porous media in the presence of gravity is presented. The scheme obtains its efficiency by using a nonlinear multigrid method to solve the system of equations resulting from a fully implicit upstream discretisation of the flow problem, and by working in a transformed coordinate frame in which the asymptotic solution is stationary. The asymptotic solution can be constructed analytically by assuming vertical pressure equilibrium and solving a one-dimensional problem. The numerical method enables us to determine the time it takes for the asymptotic solution to become a useful approximation to the actual displacement in a horizontal or slightly tilted reservoir. Some illustrative examples are given.

1. INTRODUCTION

Asymptotic solutions for two-phase displacement in two-dimensional, horizontal or slightly tilted hydrocarbon reservoirs can be constructed almost entirely analytically on the assumption of vertical pressure equilibrium (see, among others, [1,4,5,6,9,10,13,15]). These solutions are commonly used in the oil industry to obtain quick estimates of breakthrough time and production curves, when, for instance, oil is displaced by water, steam, or carbon-dioxide. They also provide the basis on which effective properties or so-called pseudo-functions are derived. In addition, the vertical-equilibrium (VE) theory can be applied to groundwater flow problems to study, for instance, the displacement of fresh by salt water. The development of the numerical scheme presented here was motivated by the question: how long does it take before the asymptotic solution becomes a valid approximation to the actual displacement process?

We will assume for the sake of exposition that the displacing fluid is water and is heavier than the fluid being displaced, namely, oil. The terms "horizontal" and "vertical" will be used to denote the along-bed and cross-bed direction of the reservoir, respectively. This implies that the gravity acceleration vector will, in general, not point in the vertical direction.

In the case of stable displacement, the competition between viscous forces and gravity will eventually result in a sharp front travelling at a fixed equilibrium angle. In the unstable case, two instabilities occur: viscous fingering and gravity tongueing. Capillary pressure suppresses viscous fingering on smaller length scales and is required from a mathematical point of view to obtain a well-posed problem. The gravity tongue will eventually override any other viscous fingers and approach an asymptotic distribution in which vertical equilibrium is attained. In both the stable and unstable case, the asymptotic solution can be computed directly by using the VE theory.

The construction method of the VE theory for unfavourable mobility ratios leads to an asymptotic saturation distribution of the form $s(x/t, y)$, as reviewed in the Appendix. This suggest the use of transformed coordinates $(t, x/t, y)$ instead of (t, x, y) for numerical computations. Because the asymptotic solution is stationary in the transformed coordinates, the time-accurate solution changes far less in time than in the inertial coordinate frame. This improves considerably the efficiency of the numerical scheme. The solution procedure is based on a nonlinear multigrid method that provides rapid convergence.

The paper is organised as follows. Section 2 lists the flow equations in the transformed domain and specifies the boundary conditions. The numerical scheme is described in Section 3. The equations are discretised in space by standard "reservoir engineering" upstream differencing and in time by a fully implicit scheme. The resulting nonlinear system of equations is solved by a Full Approximation Storage (FAS) multigrid scheme [2]. Damped Alternating Direction Line Jacobi is used as relaxation scheme, providing good convergence rates even in the case of

strong anisotropy or alignment (streamlines following gridlines), which will be predominant in the asymptotic regime.

Some numerical examples are presented in Section 4. We also give results concerning transition times in a truly horizontal reservoir for a wide range of mobility ratios and three values of the gravity number.

2. PROBLEM STATEMENT

The flow of oil and water, in the absence of wells, can be modelled by

$$\nabla . \mathcal{K}\lambda(\overline{\rho}\mathbf{g} - \nabla p) = 0, \qquad (2.1a)$$

$$\phi\frac{\partial s}{\partial t} + \nabla . \left[\lambda_w \mathbf{v}_w + \frac{\lambda_w \lambda_o}{\lambda}\mathcal{K}\nabla p_c\right] = 0. \qquad (2.1b)$$

The quantities used are:

$\mathbf{g}$	gravity acceleration vector
$\mathcal{K}(\mathbf{x})$	absolute permeability tensor
$k_o(s), k_w(s)$	relative permeability of oil and water, respectively
$p_c(\mathbf{x}, s)$	capillary pressure
p	total pressure (see [3])
s	reduced water saturation
t	time
$\mathbf{x} = (x\ y)^T$	position vector, $\mathbf{x} \in \Omega \subset I\!\!R^2$
$\lambda_o(s) = k_o/\mu_o$	relative mobility of oil
$\lambda_w(s) = k_w/\mu_w$	relative mobility of water
$\lambda(s) = \lambda_o + \lambda_w$	total mobility
μ_o, μ_w	viscosity of oil, water
ρ_o, ρ_w	density of oil, water
$\overline{\rho}(s) = (\rho_o\lambda_o + \rho_w\lambda_w)/\lambda$	average fluid density
$\phi(\mathbf{x})$	porosity
$\Omega, \partial\Omega$	domain and boundary

It is convenient to define

$$\mathbf{v}_w = \mathcal{K}(\rho_w\mathbf{g} - \nabla p), \quad \mathbf{v}_o = \mathcal{K}(\rho_o\mathbf{g} - \nabla p). \qquad (2.2)$$

The unknowns are $p(t, \mathbf{x})$ and $s(t, \mathbf{x})$. We assume the porosity and absolute permeability to be constant, the latter being

$$\mathcal{K}(\mathbf{x}) = \text{diag}\{K_1, K_2\}. \qquad (2.3)$$

In principle, we could allow for ϕ, K_1, and K_2 depending on y, but this will not be considered here.

The system of equations (2.1) can be transformed by the following coordinate transformation

$$\xi = \xi_0 + \frac{x}{\beta_0 + \beta_1 t}, \quad \eta = y, \quad \tau = t. \qquad (2.4)$$

The parameters ξ_0, β_0 and β_1 will be discussed below. The transformed gradient operator is

$$\tilde{\nabla} = \begin{pmatrix} \tilde{\partial}_1 \\ \tilde{\partial}_2 \end{pmatrix} \equiv \begin{pmatrix} (\beta_0 + \beta_1\tau)^{-1}\frac{\partial}{\partial\xi} \\ \frac{\partial}{\partial\eta} \end{pmatrix}. \qquad (2.5)$$

Equation (2.1) becomes

$$\tilde{\nabla} . \mathcal{K}\lambda(\overline{\rho}\mathbf{g} - \tilde{\nabla}p) = 0, \qquad (2.6a)$$

$$\frac{1}{\beta_0 + \beta_1\tau}\frac{\partial}{\partial\tau}\left[(\beta_0 + \beta_1\tau)\phi s\right] + \\ \tilde{\nabla} . \left[\lambda_w\mathbf{v}_w + s\mathbf{q} + \frac{\lambda_w\lambda_o}{\lambda}\mathcal{K}\tilde{\nabla}p_c\right] = 0. \qquad (2.6b)$$

Here

$$\mathbf{q} = \begin{pmatrix} -\phi\beta_1(\xi - \xi_0) \\ 0 \end{pmatrix}. \qquad (2.6c)$$

We will consider a rectangular domain $\tilde{\Omega} = [0, \tilde{L}_1] \times [0, L_2]$ in the transformed coordinates. Let $\xi_0 \in [0, \tilde{L}_1)$. A horizontal length-scale in the original coordinates is given by $L_1 = (\beta_0 + \beta_1\tau)(\tilde{L}_1 - \xi_0)$, and the corresponding domain size is $[-(\beta_0 + \beta_1\tau)\xi_0, L_1] \times [0, L_2]$. Note that L_1 is time-dependent for $\beta_1 \neq 0$.

At this point, it is convenient to introduce fluxes $\mathbf{H}^{[1]}$ and $\mathbf{H}^{[2]}$ defined by

$$\mathbf{H}^{[l]} = \begin{pmatrix} (\rho_o\lambda_o + \rho_w\lambda_w)K_l g_l - \lambda K_l\tilde{\partial}_l p \\ \lambda_w K_l(\rho_w g_l - \tilde{\partial}_l p + \frac{\lambda_o}{\lambda}\tilde{\partial}_l p_c) + \mathbf{q}_l s \end{pmatrix}, \qquad (2.7)$$

for $l = 1, 2$. The boundary conditions are chosen to be: inflow of water at the left-hand side, outflow of oil and water at the right-hand side, and impermeable rock at the bottom and top. This implies: zero flux at bottom and top side, whereas the flux at the inflow boundary is given by

$$\mathbf{H}^{[1]}_{left} = \begin{pmatrix} u_{in} \\ u_{in} \end{pmatrix}, \quad u_{in} > 0. \qquad (2.8a)$$

At the outflow boundary we specify $s = 0$ and vertical pressure equilibrium:

$$p = \rho_o g_2 \eta. \qquad (2.8b)$$

Initial conditions are chosen to be:

$$\begin{cases} s = 1, & \text{for } \xi < \xi_0, \\ s = 0, & \text{for } \xi > \xi_0, \end{cases} \qquad (2.9)$$

where $\xi_0 \in [0, \tilde{L}_1)$.

We now turn to meaning of the parameters β_0, and β_1. Suppose that the transformed domain has a fixed size $\tilde{L}_1$, and that ξ_0 is given as a reference point for the initial conditions. The initial and final length-scales in the untransformed domain are given by

$$L_1^{(i)} = \beta_0(\tilde{L}_1 - \xi_0), \\ L_1^{(f)} = (\beta_0 + \beta_1\tau^{(f)})(\tilde{L}_1 - \xi_0), \qquad (2.10)$$

for given final time $\tau^{(f)}$. Integration of equation in (2.6b) over the domain with the given boundary

conditions, under the assumption that no water crosses the outflow boundary, yields a relation for total water mass $\tilde{\mathcal{M}}_w$:

$$\frac{\partial}{\partial \tau}(\beta_0 + \beta_1 \tau)\tilde{\mathcal{M}}_w = u_{in}L_2, \qquad (2.11a)$$

where

$$\tilde{\mathcal{M}}_w \equiv \iint_{\tilde{\Omega}} \phi s \, d\xi d\eta. \qquad (2.11b)$$

In the special case that $\xi_0 = 0$ and $\beta_0 = 0$, the parameter β_1 can be expressed in terms of the PVI (Pore Volume Injected) $\tilde{P}$ in the transformed domain:

$$\beta_1 = \frac{u_{in}}{\phi \tilde{L}_1 \tilde{P}}, \quad \text{where } \tilde{P} \equiv \frac{\tilde{\mathcal{M}}_w}{\phi \tilde{L}_1 L_2}. \qquad (2.12)$$

In this case, $\tilde{P}$ is constant in the transformed domain. In the more general case, we let

$$\tilde{P} = \frac{1}{\phi(\tilde{L}_1 - \xi_0)L_2} \int_{\xi_0}^{\tilde{L}_1} d\xi \int_0^{L_2} d\eta \, \phi s, \qquad (2.13)$$

in the transformed domain. In practice, we specify the input parameters $L_1^{(i)}$, $L_1^{(f)}$, $\tilde{L}_1$, L_2, ξ_0, and $P^{(f)}$ to obtain $\tau^{(f)} = P^{(f)} \phi L_1^{(f)} / u_{in}$, and use (2.10) to find β_0 and β_1. A nonzero value of $L_1^{(i)}$ is useful in the initial phase of evolution to provide sufficient support for the pressure.

3. NUMERICAL METHOD.

A square uniform grid is chosen in the transformed domain, consisting of $N_1 \times N_2$ blocks (finite volumes). Eq. (2.6) is discretised is in space by the standard "reservoir engineering" upstream scheme and in time by a fully implicit scheme.

In discretising (2.7), the upstream switching is based on $\mathbf{v}_w$ and $\mathbf{v}_o$ to obtain upstream values for λ_w and λ_o. The term involving $\mathbf{q}$ is treated separately in an upstream manner. Finally, the capillary pressure term is discretised on a face between two blocks by evaluating $K_l \mathcal{D}(s)\nabla s$, where the non-negative coefficient $\mathcal{D}(s) \equiv -(\lambda_w \lambda_o/\lambda)dp_c/ds$ is computed for the average value of the saturations in the two neighbouring blocks.

The implicit time-discretisation leads the a system of nonlinear equations of the form

$$\begin{cases} \mathbf{r}_1(p^{n+1}, s^{n+1}) = 0 \\ \dfrac{\phi}{\Delta\tau}s^{n+1} + \mathbf{r}_2(p^{n+1}, s^{n+1}) = \dfrac{\phi}{\Delta\tau}\dfrac{\beta_0 + \beta_1 \tau^n}{\beta_0 + \beta_1 \tau^{n+1}}s^n, \end{cases} \qquad (3.1)$$

where the superscript denotes the time level, the time step $\Delta\tau \equiv \tau^{n+1} - \tau^n$, and $\mathbf{r}$ is the spatial discretisation of the divergence terms in (2.6).

The system of nonlinear equations (3.1) is solved by a multigrid method, using the Full Approximate Storage (FAS) scheme [2]. The restriction operators for the pressure p and saturation s are chosen as volume-weighted averaging. The prolongation operator is based on conservative linear interpolation.

For the multigrid solver, it is convenient to have $N_1 = 2^{M_1}$ and $N_2 = 2^{M_2}$ where M_1 and M_2 are integers. It is also convenient to have a coarsest grid that is one-dimensional in the horizontal direction, implying $M_2 \leq M_1$.

Equation (2.6a) behaves as an elliptic equation in terms of the total pressure p, whereas (2.6b) behaves as a parabolic (almost hyperbolic) equation in terms of the water saturation s. This motivates the choice of damped Alternating Direction Line Jacobi (ADLJ) as smoother. The line relaxation takes care of problems with alignment (streamlines following gridlines) and strong anisotropy. Simple Fourier analysis show that ADLJ is a good smoother for the Euler equations of gasdynamics, which are of mixed elliptic-hyperbolic type for subsonic flow [11], and also for scalar anisotropic elliptic and parabolic equations [14]. The damping factor is chosen to be 0.7, as in [14]. The smoothing scheme proceeds as follows. First, the set (3.1) of nonlinear equations is evaluated and linearised to obtain Newton's method. This results in a block pentadiagonal matrix, where a block has size 2 × 2. Then a line direction is chosen, say the ξ-direction. The off-diagonal block related to the η-direction are ignored and the resulting set of linear equations with tridiagonal matrices is solved. The solution represents a correction on the pressure and saturation and is multiplied by the damping factor before updating the pressure and saturation. The new saturation values are forced to lie in the interval $[0, 1]$. Next we repeat the entire procedure with the line the η-direction.

We use an F-cycle [2] to step through the various coarser grids. Only post-smoothing is applied, with an adaptively chosen number of smoothing steps between 3 and 6. Smoothing on a certain grid is stopped if the convergence factor of the residual per step in the maximum-norm exceeds 0.5.

The size of the time step is chosen adaptively in such a way that the change in saturation values between time steps approaches but does not exceed 0.01 in the ℓ_1-norm. In addition, if the FAS scheme does not convergence, which sometimes happens in extreme cases, the time step is halved.

Between time steps, we transform the pressure to a horizontal velocity

$$\mathbf{u}_1 = K_1[(\lambda_w \rho_w + \lambda_o \rho_o)\mathbf{g}_1 - \lambda \tilde{\partial}_1 p], \qquad (3.2)$$

using the solution and operator $\tilde{\partial}_1$ at τ^n. We then transform back to p, but now using the operator

$\tilde{\partial}_1$ evaluated at τ^{n+1}. The last transformation is implemented by starting at the outflow boundary, where the pressure is given, and then integrating back to the inflow boundary. This procedure somewhat improves the initial guess for the iteration process at time τ^{n+1}.

4. RESULTS

4.1. Parameters and functions

Before presenting some examples, we define the dimensionless parameters and specify the relevant functions. The relative permeabilities are chosen to be $k_w = s^2$ and $k_o = 1 - s$. The endpoint mobility ratio $M \equiv \lambda(1)/\lambda(0) = \mu_w/\mu_o$. The fractional flow curve $f_w = \lambda_w/\lambda$ leads to a shock speed $f'_w(s_{shock}) = M^{1/2}/(2 - M^{-1/2})$ for a shock jumping from $s = 0$ to $s = s_{shock} = M^{-1/2}$. The permeability tensor is chosen to be diagonal and isotropic: $K_1 = K_2 = k$. For the capillary pressure, we chose $p_c(s) = 3A_c s^{-1/3}$. The strength A_c can be related to a height by (A.3). A useful measure is

$$H_c = \left| \frac{p_c(1) - p_c(\frac{1}{2})}{(\rho_w - \rho_o)\mathbf{g}_2} \right|. \qquad (4.1)$$

A gravity number is defined by

$$G = |(\rho_w - \rho_o)k\mathbf{g}_2/(\mu_w u_{in})|. \qquad (4.2)$$

Time can be measured by Pore Volume Injected $P = u_{in}\tau/\phi L_1$ in the untransformed domain. Another practical measure for time is based on the horizontal distance x_p travelled by a piston-like displacement front (a straight vertical front with $s = 0$ at the right-hand and $s = 1$ at the left-hand side), scaled with respect to the reservoir height L_2:

$$T \equiv \frac{x_p}{L_2} \equiv P\frac{L_1}{L_2}. \qquad (4.3)$$

All computations were carried out on a 256×32 grid, using $\xi_0 = 0$.

4.2. Updip displacement

As a first example, we considered displacement of oil by water in a $10°$ updip reservoir, implying that both gravity components are negative. We have chosen a mobility ratio $M = 5$, gravity number $G = 2\cos 10°$, and capillary strength $H_c/L_2 = 0.1$. The evolution of the water saturation in the transformed domain is shown in Fig. 1. Also shown is the hyperbolic asymptotic result, which already agrees quite well with the true solution, except near the points where the solution approaches either pure water or pure oil.

4.3. Transition to asymptotic regime

We have studied the transition towards the asymptotic solution for a truly horizontal reservoir. The strength of the capillary pressure was taken such that $H_c/L_2 = 1.6/N_2 = 0.05$. Three values of the gravity number were used: $G = 0.1$, 1, and 10. Mobility ratios between 0.1 and 100 were chosen. Three quantities of interest have been considered: the velocity of the tip of the gravity tongue at the bottom of the reservoir, the difference between the average horizontal flux for the computed and asymptotic solutions, and the difference between production curves for the computed and asymptotic solutions.
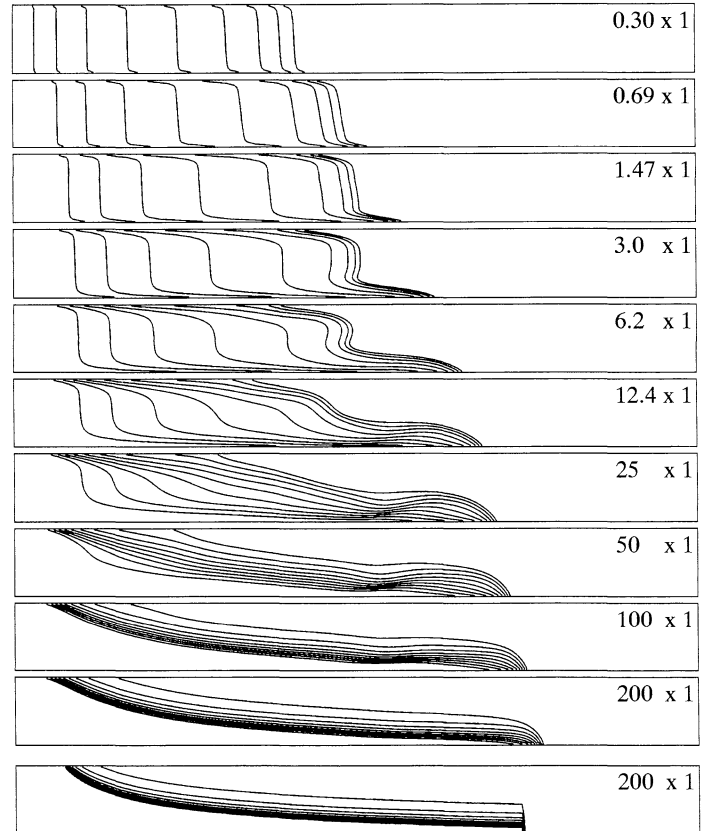

Fig. 1. *Water saturation in the transformed domain for a $10°$ updip reservoir. Shown are results for $P = 0.00034$, 0.0019, 0.0024, 0.0051, 0.011, 0.022, 0.044, 0.087, 0.17, and 0.35, from top to bottom. The true figure dimensions are given in terms of unit height. The contour values range from 0.1 to 0.9 with intervals of 0.1. The bottom figure shows the hyperbolic asymptotic solution at $P = 0.35$.*

Tip velocity. The vertical equilibrium theory leads to an average fractional flow curve $F(S)$ (A.8b), from which an effective shock speed $V = F'(S_{shock})$ can be found by solving $F'(S_{shock}) = F(S_{shock})/S_{shock}$. This will be taken as the asymptotic tip velocity. A similar quantity can be obtained from the numerical computations as follows. At a given time during the computation, we scan backwards in the horizontal direction at the bottom of the

reservoir, starting at the lowest rightmost block in the computational domain. As soon as a saturation value larger than $\frac{1}{2}s_{shock}$ (given in Sect. 4.1) is encountered, the actual horizontal position of this saturation value is determined by linear interpolation and transformed to the inertial coordinate frame, providing values x_{tip} as a function of P. Next, a least-squares fit is made of the form

$$\frac{x_{tip}}{L_1} = a_0 + a_1 P^{1/2} + a_2 P, \qquad (4.4)$$

and the asymptotic tip velocity V is taken to be a_2. Note that (4.4) contains the assumption that the evolution towards the asymptotic solution goes with the square root of time. This is suggested by analytic results for the case $k_w = s$, $k_o = 1 - s$, and $M = 1$, as presented in, e.g., [10], but has not been proven for $M > 1$. However, the assumed form (4.4) provides very accurate data fits over a fairly large time interval. The results are shown in Fig. 2 and illustrate the agreement between the numerical experiments and the VE theory. Shown is the tip velocity V as a function of the mobility ration M as obtained for the three values of the gravity number.

which the time required to reach a certain small value of this measure can be determined. The measure is based on the vertical average of the horizontal water flux.

As reviewed in the Appendix, the VE theory predicts an asymptotic average flux $\mathcal{F}^{VE}(S) = F(S)u_{in}$ for the hyperbolic asymptotic solution, or $\mathcal{F}^{VE}(S) = F(S)u_{in} + D(S)\partial S/\partial x$ for the parabolic asymptotic solution. The latter will approach the former for sufficiently large time. Here S is the vertical average of the water saturation. From the two-dimensional computations, we can compute the vertical average of the saturation S^{comp} at a given time, and the vertical average of the water flux $\mathcal{F}^{comp} \equiv \langle \mathbf{H}_2^{[1]} \rangle$, where the term due to the coordinate transformation has been set to zero ($\mathbf{q}_1 = 0$). We then determine a numerical approximation to

$$\sigma(\tau) \equiv \int_{\xi_0}^{\tilde{L}_1} |\mathcal{F}^{comp} - \mathcal{F}^{VE}(S^{comp})| \, |\frac{\partial S^{comp}}{\partial \xi}| \, d\xi, \quad (4.5)$$

using upstream differencing and the trapezoid rule. Note that $\frac{\partial S}{\partial \xi} \leq 0$ for the asymptotic solutions, but that this may not be the case for S^{comp} during of the evolution towards the asymptotic regime.
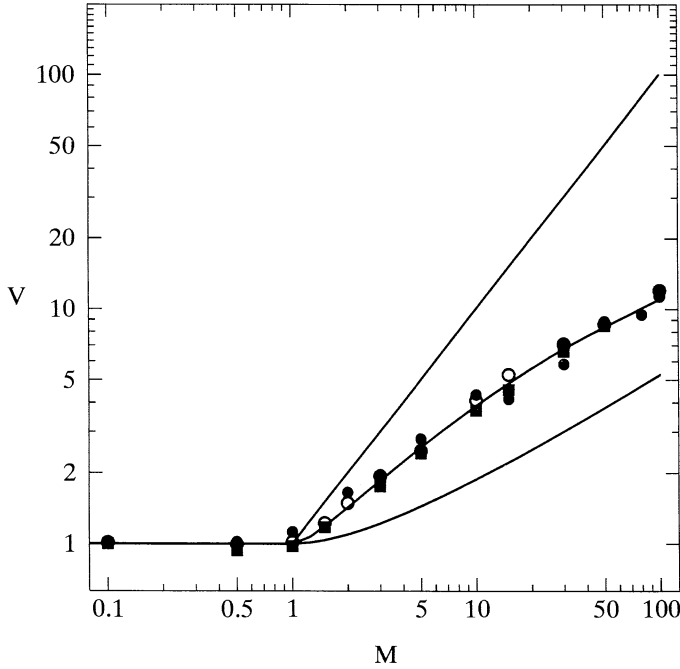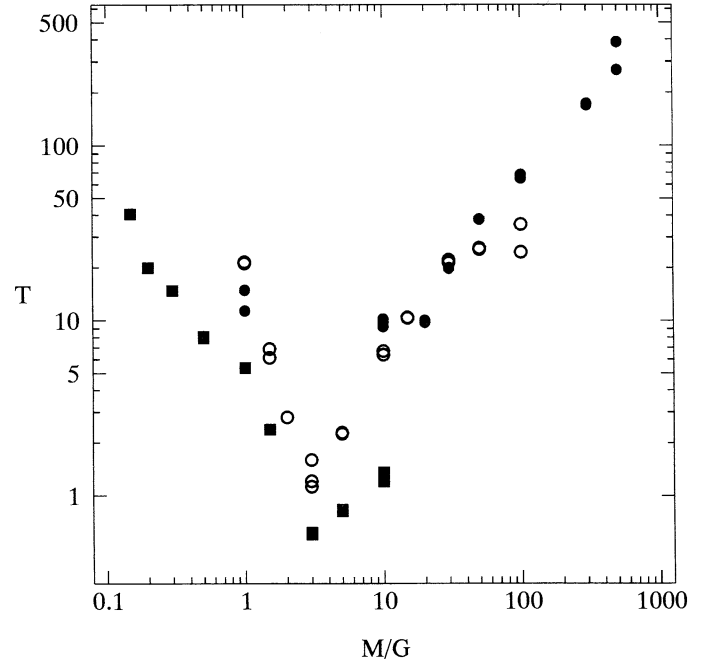

Fig. 2. *Tip velocity as a function of mobility ratio. The lines represent analytic results, using VE theory without capillary pressure (top line), with capillary pressure (middle line), and without capillary pressure and gravity (lowest line). The filled circles show computed results for $G = 0.1$, the open circles for $G = 1$, and the filled squares for $G = 10$.*

Fig. 3a. *Time needed to reach a value of σ less than 0.02, when compared to the hyperbolic asymptotic solution. The filled circles show computed results for $G = 0.1$, the open circles for $G = 1$ and the filled squares for $G = 10$.*

Transition times. We now come to the main question that motivated this work: how long does it take the solution to approach the asymptotic result? We will introduce a measure $\sigma(\tau)$ for the difference between the computed and asymptotic solution, from

After a transition period, $\sigma(\tau)$ is expected to decrease with time, although its value may never reach zero due to discretisation errors in the computed results and numerical errors in the evaluation of the asymptotic solution. A transition time T is defined somewhat arbitrarily as the time it takes for σ to

decrease to value of 0.02. Its unit is given in (4.3). Note that $\sigma(\tau)$ is not necessarily monotone, so the computations should be continued for a sufficiently long time to ensure that T is determined from a monotonically decreasing part of the graph. Figure 3 shows the transition times based on comparison of the computed solutions with either the hyperbolic or the parabolic asymptotic solutions. The data scatter has been reduced by plotting T as a function of M/G. For smaller M/G, the hyperbolic asymptotic solution provides larger transition times than the parabolic asymptotic solution, implying that the latter provides a better approximation. For larger values of M/G, on the other hand, the transition time is so large that the influence of the diffusion term in the asymptotic solution has become negligible. In this regime, we approximately have $T \simeq 0.6M/G$.
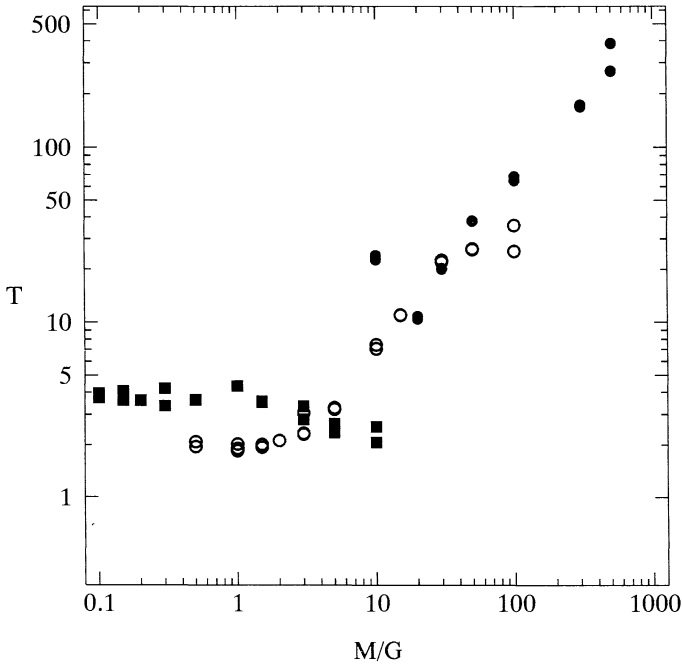

Fig. 3b. *As Fig. 3a, but for comparison to the* parabolic *asymptotic solution.*

Production curves. Another, more practical measure for comparison between computed and asymptotic solutions is the difference in oil production at a certain distance x from the inflow boundary. Let $P(x) = u_{in}t/\phi x$ be the amount of injected water, scaled with respect to the available pore volume. The cumulative amount of oil produced through a vertical section at a horizontal position x is $Q_o(t, x) = P(x) - (1/\phi x) \int_0^t dt' \mathcal{F}(t', x)$. Here $\mathcal{F}(t, x)$ denotes the vertical average of the horizontal water flux, as defined above. Using (2.1b) and the given initial and boundary conditions we find that $Q_o(t, x) = (1/x) \int_0^x dx' S(t, x')$, where $S(t, x)$ is the vertical average of the water saturation. Let

$$\delta Q(t, x) = Q_o^{comp}(t, x) - Q_o^{asy}(t, x) \qquad (4.6)$$

denote the difference between the computed and asymptotic result. For given x, we can determine the largest value of $\delta Q(t, x)$ over time, and denote this by $DQmax$. Here "largest" means the δQ which has a maximum absolute value.

Figure 4 shows $DQmax$ as a function of ML_2/Gx, using $x/L_2 = 2.5$, 5.0, 7.5, and 10, gravity numbers $G = 0.1, 1$, and 10, and a range of mobility ratios. The hyperbolic asymptotic solution has been used for Q_o^{asy}. The corresponding figure for the parabolic asymptotic solution looks roughly the same and is therefore not shown. The figure shows that VE theory can lead to an underestimation of the oil production by as much as 15%.
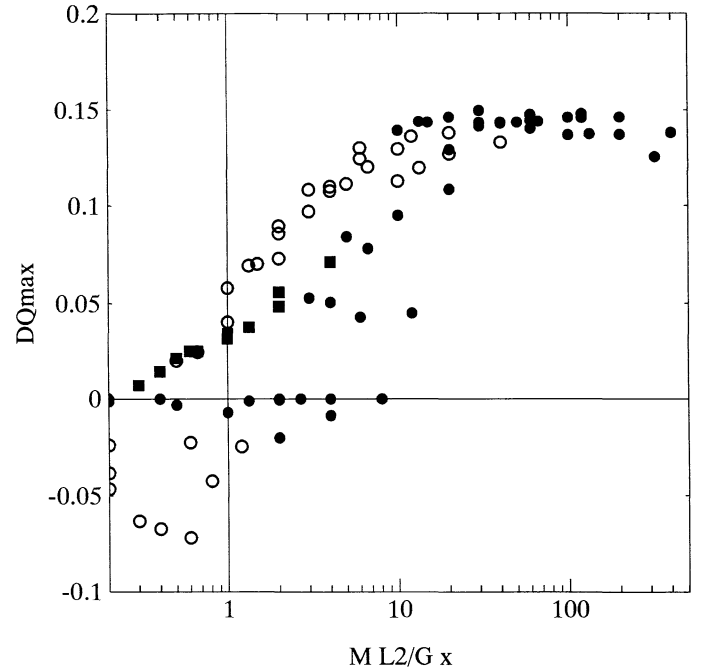

Fig. 4. *Error in cumulative oil production if the hyperbolic asymptotic solution is used.*

5. CONCLUSIONS

We have developed an efficient numerical scheme to study the evolution of stable and unstable two-phase displacement in two-dimensional, horizontal or slightly tilted reservoirs. The method obtains its efficiency by using a nonlinear multigrid solver and by working in a transformed coordinate frame in which the asymptotic solution is stationary. The multigrid method used line relaxation to deal with alignment and strong anisotropy. It typically produced a reduction of of six orders of magnitude for the residual in about 3 to 15 multigrid cycles over a wide range of parameters, even for highly unstable displacement with severe viscous fingering.

The method has been used to study the displacement of oil by water in a horizontal reservoir with constant porosity and permeability. The velocity of

the tip of the gravity tongue reaches an asymptotic value which has been shown to be in agreement with asymptotic theory. A measure has been introduced for the correspondence between the actual and the asymptotic solution. From the temporal behaviour of this measure, an effective time scale for the transition to the asymptotic regime has been determined for various values of the mobility ratio and the gravity number, but for a fixed value of the capillary number. Finally, it has been shown that the use of the asymptotic solution may lead to an error in the cumulative oil production that can be as large as 15%.

REFERENCES

[1] J. Bear, *Dynamics of Fluids in Porous Media*, American Elsevier Publ. Co., Inc., New York, 1972.

[2] A. Brandt, Lecture Notes in Mathematics **960**, Springer-Verlag, Berlin/Heidelberg/New York, 1982, pp. 220–312.

[3] G. Chavent, G. Cohen, and J. Jaffre, Computer Methods in Appl. Mechanics and Eng. **47** (1984) 93–118.

[4] K. H. Coats, R. L. Nielsen, M. H. Terhune, and A. G. Weber, SPE J. (Dec. 1967) 377–388.

[5] K. H. Coats, J. R. Dempsey, and J. H. Henderson, SPE J. (March 1971) 63–71.

[6] L. P. Dake, *Fundamentals of reservoir engineering*, Developments in Petroleum Science, Vol. 8, Elsevier Scientific Publ. Co., Amsterdam, 1978.

[7] D. N. Dietz, Proc. Kon. Ned. Acad. van Wetenschappen **B56** (1953) 83–92.

[8] C. J. van Duyn, in *Flow and Transport in Porous Media*, Proceedings of Euromech 143, Delft, September 1981, A. Verruijt and F. B. J. Barends (eds.), Balkema, Rotterdam, 1981, pp. 83–90.

[9] F. J. Fayers and A. H. Muggeridge, SPE Reservoir Engineering (Nov. 1990) 487–494.

[10] G. de Josseling de Jong, in *Flow and Transport in Porous Media*, Proceedings of Euromech 143, Delft, September 1981, A. Verruijt and F. B. J. Barends (eds.), Balkema, Rotterdam, pp. 75–82.

[11] W. A. Mulder, SIAM J. Sci. Stat. Comput. **11** (1990) 389–397.

[12] W. Proskurowski, J. Comput. Phys. **41** (1981) 136–141.

[13] J. W. Sheldon, and F. J. Fayers, SPE J. (Sept. 1962) 275–282.

[14] P. Wesseling, Int. Series of Numerical Math. **98** (1991) 105–127.

[15] Y. C. Yortsos, SPE paper No. 22612, presented at the 66th Annual Technical Conference and Exhibition of the SPE, Dallas, Texas, October 1991.

APPENDIX: Asymptotic solutions

Here we review the construction method for the asymptotic solution. The assumption of vertical equilibrium is satisfied by

$$\frac{\partial p}{\partial y} = \bar{\rho}\mathbf{g}_2, \qquad \frac{\partial p_c}{\partial y} = -\Delta\rho\,\mathbf{g}_2, \qquad (A.1)$$

where $\Delta\rho \equiv \rho_w - \rho_o$. Integration of the pressure yields

$$p = \bar{\rho}\mathbf{g}_2 y - \psi(x). \qquad (A.2)$$

The capillary pressure becomes

$$p_c(s) = p_c(s_1) - \Delta\rho\,\mathbf{g}_2(y - y_1(t, x)). \qquad (A.3)$$

Because p_c depends on s, (A.3) implicitly determines a cross-bed saturation profile, with $s = s_1$ as some reference saturation. It is assumed that $dp_c/ds < 0$ and $p_c(s)$ is bounded for $s \in (0, 1)$. If $p_c(0)$ is bounded, then the saturation profile can be extended by $s = 0$ in the proper y-direction. Otherwise, s never reaches zero, although it may become arbitrary small. Similarly, if $p_c(1)$ is bounded, the saturation profile can be continued by $s = 1$ in the opposite direction. Note that, in general, $y_1(x)$ does not have to lie in the interval $[0, L_2]$, but y does.

Substitution into (2.1) leads to

$$\frac{\partial}{\partial x}K_1\lambda(\bar{\rho}\gamma + \frac{\partial\psi}{\partial x}) = 0,$$
$$\phi\frac{\partial s}{\partial t} + \frac{\partial}{\partial x}K_1\lambda_w(\rho_w\gamma + \frac{\partial\psi}{\partial x}) = 0, \qquad (A.4)$$

where $\gamma \equiv \mathbf{g}_1 + \mathbf{g}_2 dy_1/dx$.

A cross-bed averaging operator is defined by

$$\langle\cdot\rangle \equiv \frac{1}{L_2}\int_0^{L_2}(\cdot)dy. \qquad (A.5)$$

Application to (A.4) leads to

$$\frac{\partial}{\partial x}K_1[(\langle\lambda_w\rangle\rho_w + \langle\lambda_o\rangle\rho_o)\gamma + \langle\lambda\rangle\psi_x] = 0, \qquad (A.6a)$$

$$\phi\frac{\partial S}{\partial t} + \frac{\partial}{\partial x}K_1[\langle\lambda_w\rangle\rho_w\gamma + \langle\lambda_w\rangle\psi_x] = 0, \qquad (A.6b)$$

using the no-flow boundary conditions at $y = 0$ and $y = L_2$. Here $S \equiv \langle s\rangle$. The first equation is solved by

$$K_1[(\langle\lambda_w\rangle\rho_w + \langle\lambda_o\rangle\rho_o)\gamma + \langle\lambda\rangle\psi_x] = u_{in}, \qquad (A.7)$$

from which ψ_x can be obtained. Substitution in (A.6b) yields

$$\phi\frac{\partial S}{\partial t} + \frac{\partial}{\partial x}\Big[F(S)u_{in} + D(S)\frac{\partial S}{\partial x}\Big] = 0, \qquad \text{(A.8a)}$$

where the average fractional flow curve

$$F(S) = \frac{\langle\lambda_w\rangle}{\langle\lambda\rangle}[1 + \langle\lambda_o\rangle\,\Delta\rho\,K_1\mathbf{g}_1/u_{in}], \qquad \text{(A.8b)}$$

and the diffusion coefficient

$$D(S) = \frac{\langle\lambda_w\rangle\langle\lambda_o\rangle}{\langle\lambda\rangle}K_1\frac{dP_c(S)}{dS}. \qquad \text{(A.8c)}$$

Here we have introduced an average capillary pressure $P_c(S)$ by letting

$$\frac{dP_c(S)}{dS} \equiv \Delta\rho\,\mathbf{g}_2\frac{dy_1}{dS}. \qquad \text{(A.8d)}$$

The diffusion term leads to evolution with a length scale proportional to $t^{1/2}$, whereas the hyperbolic convection term described by $F(S)$ has a length scale proportional to t. For sufficiently large time, the latter will dominate the $O(t^{1/2})$ term and a purely convective equation remains. This equation can be solved by the usual procedure for Riemann problems, for a left saturation $S = 1$ and right saturation $S = 0$ [12]. The fractional flow curve $F(S)$ is replaced by its convex hull $F^H(S)$ and the solution is given implicitly by

$$x(S) = t\frac{u_{in}}{\phi}\frac{dF^H(S)}{dS}. \qquad \text{(A.9)}$$

For given x and $S = \langle s\rangle$, Eq. (A.3) can then be used to reconstruct $s(x/t, y)$. An example of this procedure can be found in [6].

In practice, the asymptotic solution is evaluated numerically. First a suitable set of values for y_1 is chosen. Next, a table with these values and the corresponding $S = \langle s\rangle$, λ_w, and λ_o is constructed, from which $F(S)$, $D(S)$, and $dF^H(S)/dS$ are determined. This requires the inversion of $p_c(s)$ and involves some numerical integration and differentiation. Once this table is constructed, the computation of the asymptotic solution (A.9) based on $F(S)$ boils down to table look-up and interpolation. We will refer to this solution as the *hyperbolic* asymptotic solution. Alternatively, we can solve the one-dimensional convection-diffusion equation numerically by integrating in time in a manner similar to the method described in Section 3. We will refer to this solution as the *parabolic* asymptotic solution. The latter should approach the former for sufficiently large time.

We end this Appendix by giving some examples for simple cases.

Fully segregated flow. If the capillary pressure becomes vanishingly small, Equation (A.3) implies that the vertical transition zone between $s = 1$ and $s = 0$ has zero length, and we have fully segregated flow. Then y_1 represents the cross-bed water height and

$$S = \frac{y_1}{L_2}, \quad \langle\lambda_w\rangle = S/\mu_w, \quad \langle\lambda_o\rangle = (1-S)/\mu_o. \quad \text{(A.10)}$$

Define dimensionless (but signed) gravity numbers

$$G_l \equiv \frac{K_1\Delta\rho g_l}{\mu_w u_{in}}, \quad (l = 1, 2). \qquad \text{(A.11)}$$

Then

$$F(S) = \frac{S}{MS + (1 - S)}[M + G_1(1 - S)],$$
$$D(S) = u_{in}G_2 L_2\frac{S(1 - S)}{MS + (1 - S)}. \qquad \text{(A.12)}$$

For $M = 1 - G_1$, we have $F(S) = S$. For $M < 1 - G_1$, the convex hull $F^H(S) = S$. In all these cases, Eq. (A.9) leads to piston-like displacement. For $M > 1 - G_1$, the convex hull $F^H(S) = F(S)$ and Eq. (A.9) describes a gravity tongue:

$$\frac{y_1}{L_2} = S(x/t) = \frac{1}{M - 1}\left(-1 + \sqrt{\frac{M(M - 1 + G_1)}{G_1 + (M - 1)\zeta}}\right), \qquad \text{(A.13a)}$$

where

$$\zeta = \frac{\phi}{u_{in}}\frac{x}{t} \in [\frac{1 - G_1}{M}, M + G_1]. \qquad \text{(A.13b)}$$

Note that the diffusion term has been ignored in these results.

Travelling waves. We consider fully segregated flow but do not ignore the diffusion term. For $M \leq 1 - G_1$, a travelling wave solution exists of the form $S(x')$, with $x' = x - u_{in}t/\phi$. Substitution of this expression into (A.8a) leads to

$$u_{in}\frac{S(1 - S)}{MS + (1 - S)}(M - 1 + G_1 + G_2 L_2\frac{dS}{dx'}) = 0, \qquad \text{(A.14)}$$

implying that

$$\frac{y_1}{L_2} = S(x') = \left(\frac{1 - G_1 - M}{G_2 L_2}\right)x'. \qquad \text{(A.15)}$$

This represents a linear front at a fixed angle moving with constant speed. Note that (A.9) ignores the diffusion term and predicts a vertical front.

Miscible horizontal displacement. For $M = 1$, $G_1 = 0$, and $p_c(s) \to 0$, a solution of (A.8a) is

$$\frac{y_1}{L_2} = S = \frac{1}{2}\left[1 - x'\sqrt{\frac{-\phi}{G_2 L_2 u_{in}t}}\right], \qquad \text{(A.16)}$$

if $G_2 < 0$ [8]. This represents a linear front moving with constant speed and becoming more and more horizontal as time progresses.